NON-STATIONARY DYNAMIC ANALYSIS OF A WIND TURBINE POWER DRIVETRAIN: OFFSHORE CONSIDERATIONS

F. Viadero, A. Fernández*, M. Iglesias, A. de-Juan, E. Liaño, M.A. Serna

Department of Structural and Mechanical Engineering, University of Cantabria. Avda. de los Castros s/n 39005 Santander, Spain.

Corresponding Author
Tel +34 (942) 20 09 36
Fax +34 (942) 20 18 53
fernandra@unican.es

Abstract

This paper presents a multi-body model for studying the non-stationary dynamic behaviour of a wind turbine power drivetrain. The model includes some offshore considerations, such as the extra degrees of freedom and boundary conditions that installation on an offshore floating platform can add. The studied problem is an offshore implementation, with seafloor depths of the order of a hundred meters, making it necessary to use a floating platform. Special attention is paid to the characteristics of the combined offshore buoy support and detailed model of the power train, in order to assess the impacts of buoy movement on forces on gears and bearings. A multi-body analysis code was used to develop the model, and a conventional wind turbine set-up was implemented as an example. Gearbox dynamic behaviour was simulated for common manoeuvres such as a start-up and an emergency stop, and the results are presented and discussed.

KEYWORDS

Wind turbine, Offshore, Gear dynamics, Meshing stiffness

1 INTRODUCTION

Wind energy development has been of great importance in the last decade. Many offshore wind farms have been built, but the majority of these are close to the coast, where the shallow water allows the wind turbine to be anchored to the sea bed. To minimize the visual impact of these farms and to increase the installed power, turbines are now being installed far from the coast, where they cannot be seen and where the wind speed is higher. The alternative to anchoring in these deep sea areas is to use floating structures that support the wind turbine, usually consisting of a buoy that gives vertical stability to the wind turbine and chains that limit the horizontal displacements. These conditions represent a new engineering challenge from the point of view of the structural elements but also for the gearbox design, as the dynamic loads are more complex than those corresponding to conventional grounded facilities. This is due to the coupling between the structural motions (much larger than the onshore deflections) and

the wind and wave loads, and also because the rotor is subjected to significant angular displacements which generate gyroscopic effects and loading [1].

The gearbox is one of the most critical components in the operation of wind turbines, being responsible for most of the downtime and consequential increases in operational costs [2]. This issue has received the attention of several researchers, and more accurate and advanced models have been developed in recent years to help understand the dynamic loads at the level of gearbox components.

One of the most important phenomena involved in the dynamic behaviour of gear transmissions is related to the parametric excitation arising from variable meshing stiffness. This phenomenon can be approached with formulations of different complexity, ranging from simple models based on lumped parameters [3] to advanced contact models based on hybrid formulations combining numerical and analytical tools [4]. Nevertheless, it has been proved that lumped mass models can provide a clear picture of the rich, dynamic behaviour, even replicating experimental results under non-resonance conditions, but overestimating the dynamic factors when close to resonance [5]. In the particular case of planetary transmissions, Ambarisha et. al [6] extended the analysis of different modelling approaches and concluded that lumped models can also be useful when they account for varying meshing stiffness.

Bearings are another component which must be considered. In fact, bearings have a similar behaviour to the gears, as they also present varying compliance due to the change in the number of rolling elements supporting the load. However, the most common modelling approach is to represent the bearing by a time-invariant stiffness and damping matrix, as was done in [7-8] where the flexibilities of shafts, carriers and even the supporting structure were also considered.

Although various studies have addressed the dynamic modeling of floating offshore wind turbines [9], the complexity of a model which would provide realistic results makes it impossible from the point of view of computational effort to perform dynamic analysis with focus on subsystem levels such as the gearbox. This is why most research on wind turbine gearboxes is approached instead by means of field-test programs (NREL projects), which are less reliant on dynamic complete system models (because of the simplifications required in order to be functional). Nevertheless, some work has recently been published on the specific topic of gearboxes in floating platform turbines, combining a multibody model of the gear drive with a previous coupled wind-wave analysis [10], which calculates the loads on the main shaft of the drivetrain and the movement of the nacelle. These authors also carried out a model fidelity study, concluding that gear tooth and bearing compliances, together with shaft flexibility characteristics, are a sufficient level of detail for predicting the internal loads in the drivetrain. Unfortunately, the computational effort for this approach is still large, needing up to three days for a 1-hour real-time simulation. More recently, Guo et al. [11] carried out a similar model fidelity study for transient loads, concluding that a fully-rigid gearbox model with tooth compliance (like the one presented in this work) can be used when the interest is focused on gear contact forces, while the bearing loads are overestimated by up to a 20%. In these models the calculation times are reduced drastically, such that they are a powerful tool for identifying potential problems during the design stage and also for parametric studies or optimization purposes.

This work focuses on the non-stationary behaviour of the power drivetrain model of a wind turbine, including some features schematically representing the offshore effects. The turbine has free movements in all displacements and rotations, with the mooring lines and the floating structure affecting the overall behaviour of the drivetrain. With this aim, a model has been developed using a Multibody System (MBS) code which allows a clear and simple handling of the whole system. Moreover, the MBS approach provides more flexibility, for example it allows additional phenomena to be included, such as the excitations coming from aerodynamic blade loads or the flexibility of different components (shafts, tower, etc.). However, in this study attention is focused on the dynamics of the gear drivetrain model, noting that some important features of the offshore wind turbines are not implemented (such as the coupled wind-wave effects).

The model developed includes a planetary and two ordinary stages with variable meshing stiffness as well as bearing flexibility. Special attention is given to the start-up and emergency stop manoeuvres, as dynamic loads are critical in these types of operations.

2 MBS MODEL

The MBS model was developed entirely in MSC-ADAMS and is presented in Figure 1, where details of the gearbox and a kinematics scheme are shown. The blades and the hub are considered as rigid bodies with lumped mass and inertia. Wind loads are included as external forces on the rotor hub, thus neglecting aerodynamic loads due to the structural behaviour of the blades and the aero-elastic coupling. Buoy restoring forces are included at the base of the tower using specific single forces defined in the MBS code environment. Although this is a rather simplified model of the buoy, the aim of this work focuses on the analysis of the drivetrain dynamic response. Thus, angular motions and gyroscopic loads are taken into account during non-stationary manoeuvres. The gearbox shafts and gears are lumped and assumed to be rigid bodies, while gear meshing forces are modelled by a variable-stiffness spring following the approach described later. The rotor hub is connected through the main shaft to the carrier of the planetary stage (see Figure 1). The carrier rotates with the planets and transmits the power to the low speed shaft via the sun gear. Then, two ordinary stages are used to increase the rotational speed, up to the desired value at the generator side, where the generator is modeled as a representative mass.

For the sake of simplicity, and with the aim of reducing the computational effort, all shafts are considered as rigid. This approach is commonly used [12, 13] because it provides a good level of detail of the drive dynamics, particularly with respect to the excitation of drivetrain frequencies during transient manoeuvres. On the other hand, the main shaft does have flexible bearings, which are included in the MBS model as bushing joints with corresponding stiffness and damping values.

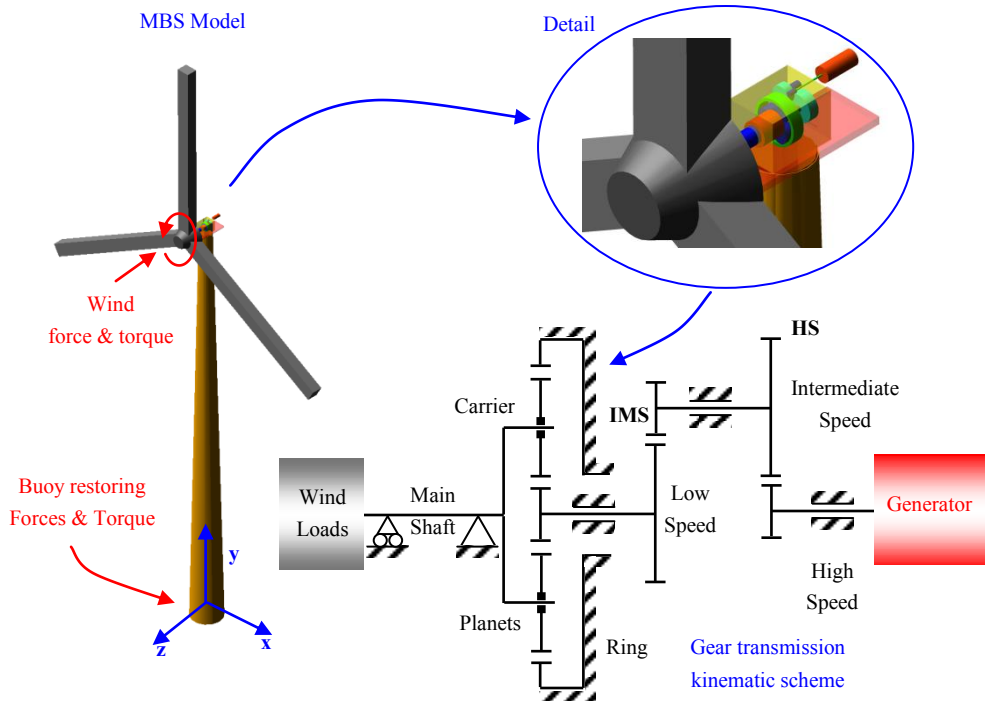

Figure 1. MBS model and details of the drive train

The torque load due to the generator (TG) is implemented by a simple induction generator model [14] according to the expression

$$T_G = R_T(\omega_S - \omega) \qquad (1)$$

where ω is the actual generator speed, ω_S is the synchronous generator speed corresponding to the zero torque value and R_T is a constant defined to balance the nominal wind torque at the desired operational speed ω_G. This model is connected when the generator rotational speed reaches a certain value defined by the user. In this way the coupling can be included even if the generator is working as a motor, when the generator speed is lower than the synchronous speed.

Meshing forces have been included as user functions (GFORCE), defined following the approach described in a previous work by the same authors for a low speed ordinary transmission [3]. Tooth contacting forces are assumed to be contained in the transmission plane and always perpendicular to the tooth surface. Thus, tooth deflection can be obtained from the relative displacements of each gear center x_i, y_i, z_i, θ_{xi}, θ_{yi}, θ_{zi}, (see Figure 2), using the following expression:

$$\begin{aligned}\delta ij = &(x_i\cos\varphi_{ij} + y_i\sin\varphi_{ij} + \rho_i\theta_{zi} - x_j\cos\varphi_{ij} - y_j\sin\varphi_{ij} + \rho_j\theta_{zi})\cos\beta_{ij}\frac{1}{2} \\ &+(z_i - \rho_i\theta_{xi}\cos\varphi_{ij} - \rho_i\theta_{yi}\sin\varphi_{ij} - z_j - \rho_j\theta_{xj}\cos\varphi_{ij} - \rho_j\theta_{yj}\sin\varphi_{ij})\sin\beta_{ij} + e_{ij}(t)\end{aligned} \qquad (2)$$

where $e_{ij}(t)$ represents the periodic static transmission error due to profile errors, β_{ij} is the helix angle on the pitch cylinder, φ_{ij} the normal pressure angle and ρ_i and ρ_j are the base radii of gears i and j.

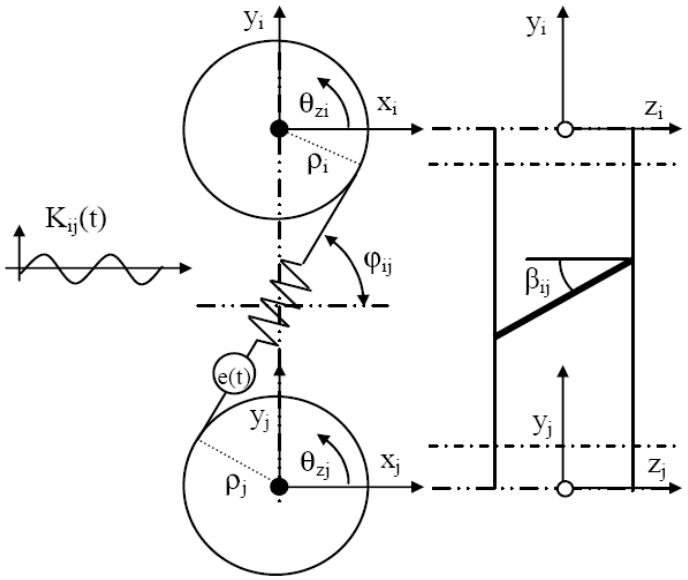

Figure 1. Tooth meshing deflections

Once tooth deflections are known, meshing forces are obtained by multiplying the resulting deflections by the gear pair stiffness as follows:

$$
\begin{aligned}
F_{Xi} &= -\delta_{ij}\cdot K_{ij}\cdot \sin\varphi_{ij}\cdot\cos\beta_{ij} & F_{Xj} &= \delta_{ij}\cdot K_{ij}\cdot \sin\varphi_{ij}\cdot\cos\beta_{ij}\\
F_{Yi} &= -\delta_{ij}\cdot K_{ij}\cdot \cos\varphi_{ij}\cdot\cos\beta_{ij} & F_{Yj} &= \delta_{ij}\cdot K_{ij}\cdot \cos\varphi_{ij}\cdot\cos\beta_{ij}\\
F_{Zi} &= \delta_{ij}\cdot K_{ij}\cdot \sin\beta_{ij} & F_{Zj} &= -\delta_{ij}\cdot K_{ij}\cdot \sin\beta_{ij}\\
T_{Xi} &= -\delta_{ij}\cdot K_{ij}\cdot \rho_i\cdot \sin\varphi_{ij}\cdot\sin\beta_{ij} & T_{Xj} &= -\delta_{ij}\cdot K_{ij}\cdot \rho_j\cdot \sin\varphi_{ij}\cdot\sin\beta_{ij}\\
T_{Yi} &= -\delta_{ij}\cdot K_{ij}\cdot \rho_i\cdot \cos\varphi_{ij}\cdot\sin\beta_{ij} & T_{Yj} &= -\delta_{ij}\cdot K_{ij}\cdot \rho_j\cdot \cos\varphi_{ij}\cdot\sin\beta_{ij}\\
T_{Zi} &= -\delta_{ij}\cdot K_{ij}\cdot \rho_i\cdot \cos\beta_{ij} & T_{Zj} &= -\delta_{ij}\cdot K_{ij}\cdot \rho_j\cdot \cos\beta_{ij}
\end{aligned}
\qquad (3)
$$

The approach used in this work allows for the consideration of meshing non-linearity, such as the backlash [15]. Several studies have considered variations in meshing stiffness K_{ij} along the contact point to take into account the number of tooth couples in contact for each position. In this case, due to the high contact ratio, there is a large overlapping of tooth couples; therefore, the stiffness can be described in a simple expression defined by a mean value K_{mij} and the first harmonic term of amplitude A_{ij} [3] as:

$$K_{ij}(t) = K_{m_{ij}} + A_{ij}\cdot\sin(2\pi f_{si} Z_i + \upsilon_{ij}) \quad (4)$$

where f_{si} is the shaft rotational frequency, Z_i is the gear teeth number and υ_{ij} the phase. The stiffness variations calculated following Cai's approach [16] for a meshing period can be observed in Figure 3, where the individual contributions of each contact pair (K_1, K_2 and K_3) along a mesh period are also represented. In Figure 3b, details of the total stiffness and the harmonic approximation are shown, to illustrate the negligible error caused by the assumption in (4).

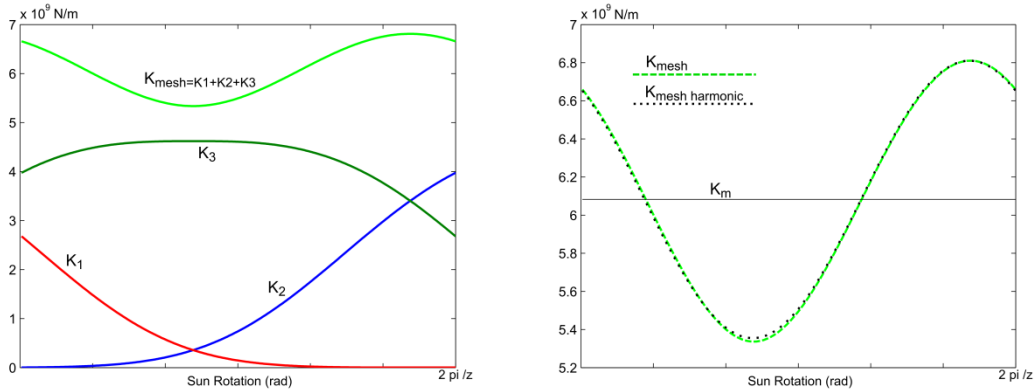

Figure 3. Meshing stiffness for the gear pair Planet/Sun for a meshing period

The floating support platform is a spar-buoy concept which achieves static stability by locating the center of gravity far below the center of buoyancy by means of ballast. Three catenary mooring lines in a delta connection are used to attach the buoy to the sea floor, thus restricting horizontal movement of the turbine within a certain area. The disposition of the chains around the floating platform defines the yaw stiffness, which is one of the more critical design features for this kind of support. A preliminary analysis of the hydrostatic buoyancy behaviour yields the rotational stiffness as well as the translational stiffness in the vertical direction.

Interest in the hydrodynamic forces is focused on the analysis of the transient operations, particularly the gyroscopic effects related to pitch rotation, as well as the consequences of variable stiffness and reverse contacts. No excitations arising from wave forces were considered. By contrast, buoy mass and inertia were increased in order to include the effects of the fluid mass attached to the platform, and hydrodynamic damping was also included in the MBS model by means of the GFORCE element.

The mooring lines were analysed offline for horizontal displacements and the resulting forces and displacements were stored to obtain the equivalent stiffness. Then, three non-linear springs were arranged in the MBS model in the xz plane, configured such that they were 120 degrees out of phase (see Figure 4).

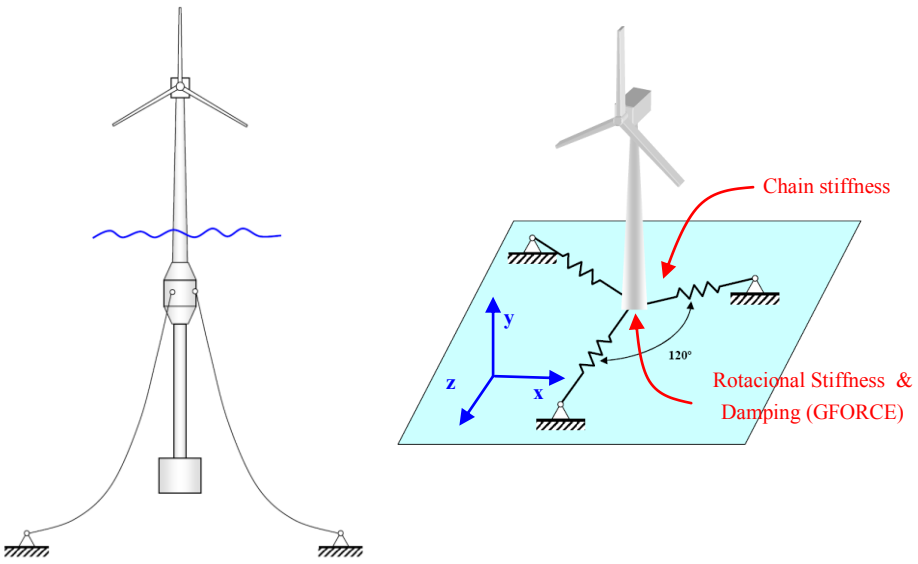

Figure 4. MBS model of the buoy restoring forces

3 APLICATION EXAMPLE

The MBS model described above was applied to a known wind turbine drive train of 750 kW, specifically the NREL 750 GRC [17]. The details, parameters and data related to this example which have not previously been described in the cited reference are highlighted in this work. In Table 1 the data corresponding to the meshing stiffness of each gear pair are presented. These data were obtained following the approach proposed in [3]. Bearings for the main shaft were modelled as BUSHING joints. The axial stiffness for this bearing was given the same value as that used for the radial direction, of 10^9 N/m.

Table 1 Transmission gear data

	Transversal Contact ratio	*Axial Contact ratio*	*Average Stiffness (N/m)*	*Variable Stiffness (N/m)*
Planet / Ring	1.5847	1.2456	$5.7605\ 10^9$	$6.287\ 10^8$
Planet / Sun	1.5456	1.2456	$6.0827\ 10^9$	$7.276\ 10^8$
IMS Gear Pair	1.5208	1.8668	$2.9956\ 10^9$	$3.468\ 10^8$
HS Gear Pair	1.4538	2.1562	$1.7947\ 10^9$	$1.809\ 10^8$

In the model of the floating structure, the vertical translation stiffness due to the combination of gravitational forces and flotation was linearized for the nominal buoyancy level and assigned a value of 96.74 kN/m. A schematic displaying the most important data related to the geometry of the buoy platform is presented in Figure 5.

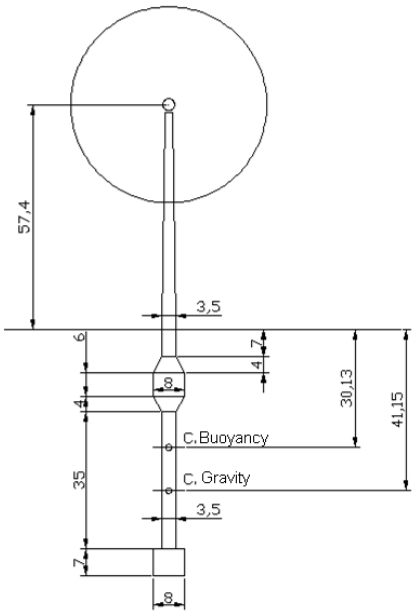

Figure 5. Buoy main dimensions

The horizontal stiffness due to the tension of the mooring lines is non-linear and described by the values shown in Table 2, which are also represented in Figure 6. In the same Figure, the non-symmetric stiffness behaviour due to the mooring line

arrangement is presented. In the present study, wind acts on the line with the greatest stiffness. In order to simplify the model, the same values have been used for roll, pitch and yaw rotational stiffness. Moreover, linear viscous damping has been considered for all buoy degrees of freedom (see Table 2).

Table 2 Parameters of the wind turbine

	Stiffness (15 m)	***Stiffness (20 m)***	***Stiffness (25 m)***	***Damping***
Horizontal translation (for 15m, 20m, 25m)	16.34 kN/m	23.52 kN/m	39.2 kN/m	40 kN/m/s
Vertical translation	96.74 kN/m	96.74 kN/m	96.74 kN/m	40 kN/m/s
Roll / Pitch / Yaw	114 MNm/rd	114 MNm/rd	114 MNm/rd	1 MNm/rd/s

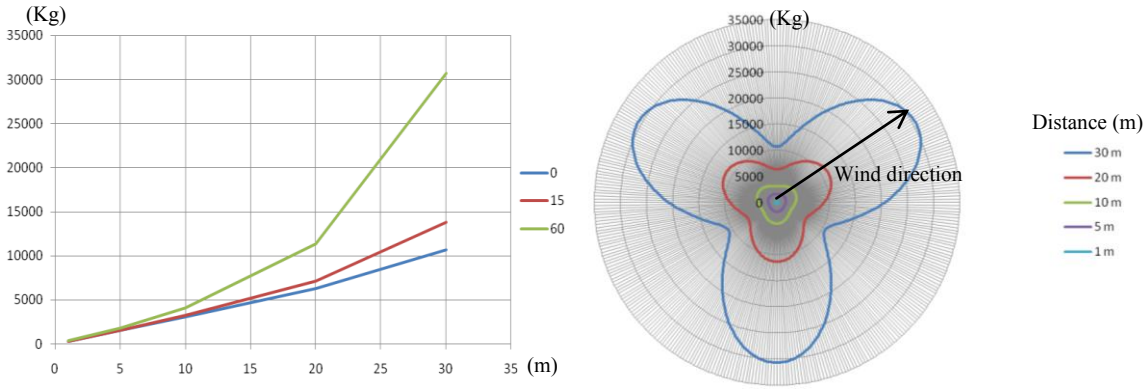

Figure 6. Non-linear relationship between horizontal buoy displacement and mooring line forces

The results presented below correspond to the previously described model under several transitory loads, which are graphically represented in Figure 7 in six sketches showing time, mooring line deflections, and forces on the system. The forces include wind effects, braking forces (both mechanical and aerial), and generator torque.

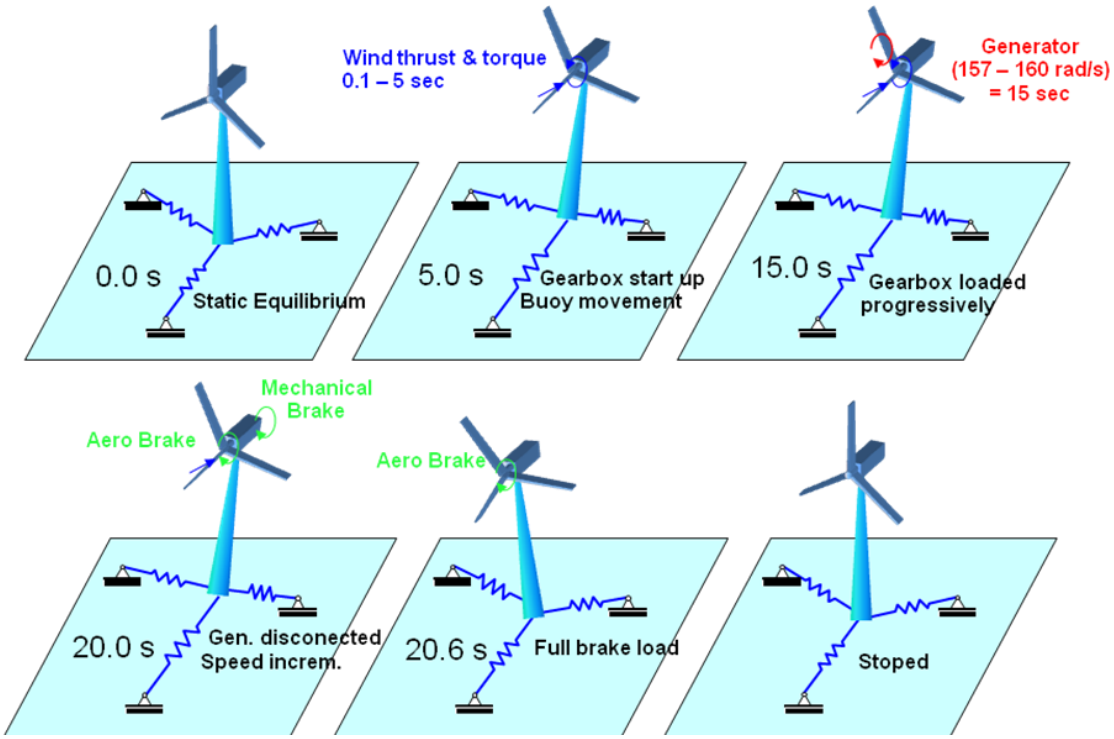

Figure 7. MBS model of the buoy restoring forces

Initially, with the generator disengaged, the model was subjected to wind loads on the blades which are represented as a torque and a thrust force applied to the hub rotor. Load magnitudes were incremented progressively from zero to the maximum value for the time period, ranging from 0.1 to 5 seconds. As a consequence of this load, the drivetrain started up and simultaneously the floating support began its horizontal movement as well as a pitch oscillation due to the wind thrust load.

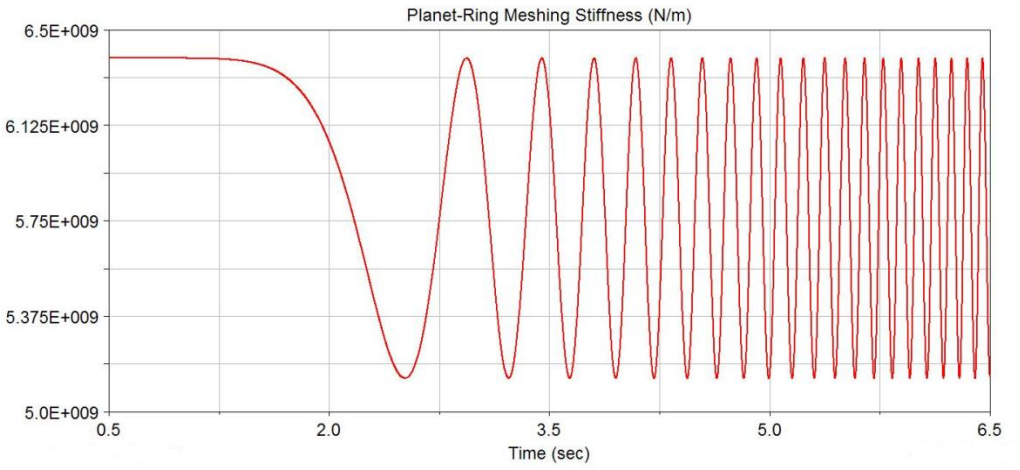

Figure 8. Detail of the variable meshing stiffness during the run-up

Later, when the rotational speed of the high speed shaft reached the 157 rad/s level, the generator was connected progressively, achieving maximum power when the speed reached 160 rad/s. Then, after a short period of time, the turbine entered its stationary working conditions of torque load and rotational speed. The next event in the simulation

was an emergency stop manoeuvre due to electrical failure, with the aim of studying the phenomena associated with an unexpected shutdown of the machine and an evaluation of the contact stresses in the gears and bearings, as well as the dynamic behavior of the entire machine. This event was simulated by disconnecting the generator (in second 20) with a sudden drop in the resistant torque. As a consequence of this the drive train lost the pretension in the meshing contacts, increasing their speed. After 0.1 seconds (second 20.1) the control system reacted, activating the aerodynamic brake by pitching the blades. Then, up to second 25, the torque and thrust due to the wind were progressively reduced and simultaneously a rotational damper representing the aerodynamic brake torque was connected in the hub. Furthermore, at the same instant (second 20.1), the mechanical brake was activated in the generator side, with the braking force increasing to a maximum after a further 0.5 seconds (second 20.6). Finally, the torque of the mechanical brake was progressively reduced as a function of the generator speed, from 10 rad/s to 1 rad/s when it was finally disengaged.

Figure 8 shows the evolution of the meshing stiffness for the planet-ring contact during start-up. In Figure 9 a) the wind effects in terms of thrust and torque are presented. It should be noticed that in the case of the wind torque, the value presented corresponds to the absolute torque, and that its sign changes with the activation of the aerodynamic brake at second 20.1. Figure 9 b) shows the loads on the generator side together with its angular velocity. The red line shows the generator torque as well as the mechanical brake: in this case the sign remains constant as the mechanical brake substitutes the effect of the faulty generator.

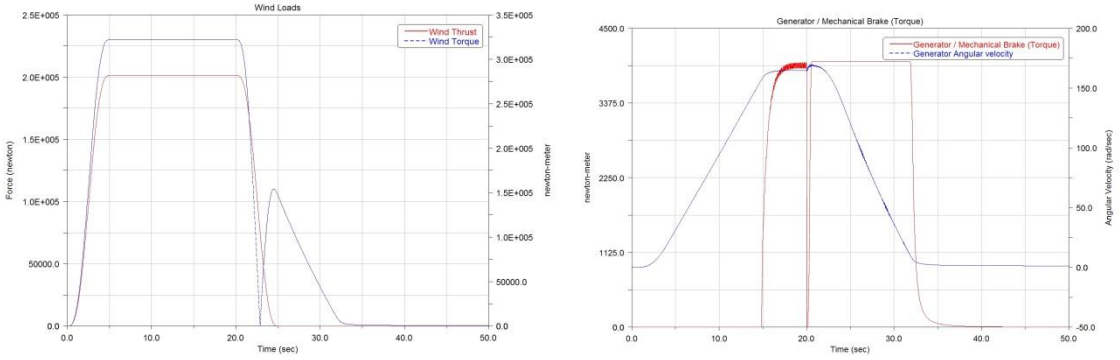

Figure 9. **a) Wind loads** **b) Generator/brake torque**

In Figure 10 a) the most significant displacements regarding the floating platform motion are presented: the pitch amplitude reached a maximum at 10.64 degrees (the initial position for t=0 s was vertical), while the horizontal amplitude in the wind direction reached 25 m. The most important consequence of the pitch motion was the resulting increase in the main bearing load in the radial direction, due to the gyroscopic torque, as is evident in Figure 10 b). Of particular note, the greatest loads found in the application example were during the start-up manoeuvre rather than the emergency shutdown phase (this may depend on the control system applied).

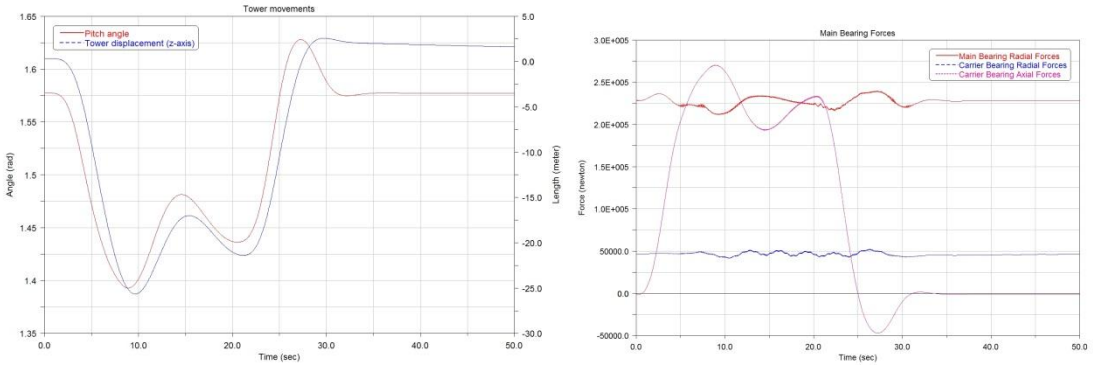

Figure 10. **a) Tower movements** **b) Main bearing forces**

Regarding the drivetrain internal behaviour, Figure 11 shows the meshing deformation for both meshing types: internal (ring-planets) and external (sun-planets). In this figure it can be seen how the gears experienced counter-flank contact (negative meshing deformations) during the start-up operation. This phenomenon was caused by the flexibility of the main shaft bearings: the rotor weight introduced a pitch movement which was transmitted to the planets and induced these counter-flank contacts. As the transmitted torque increased, this phenomenon disappeared. Counter-flank contacts also occurred just at the disconnection of the generator, as a consequence of the pretension lost in the drive train meshing contacts.

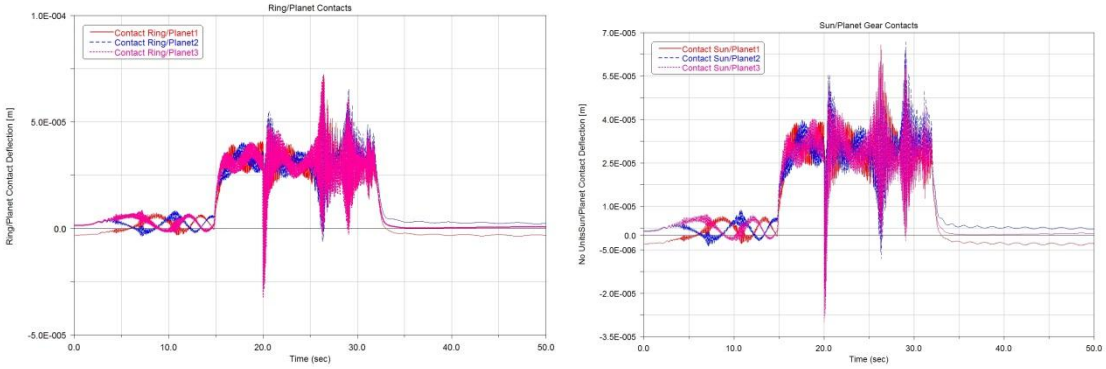

Figure 11. **a) Ring/Planet contact deflection** **b) Sun/Planet contact deflection**

Both during start-up and the emergency brake, the excitation of one drivetrain resonance frequency was found at low frequencies. At these times, the amplitudes of the contact deformation and bearing/meshing forces were incremented. This is shown in more detail in Figure 12, where a waterfall spectrum of the high-speed gear stage deflection derivative is shown. This spectrum reveals resonance at a frequency of approximately 10 Hz. A global modal analysis of the system allowed the identification of this resonance as a pitch mode of the main rotor.

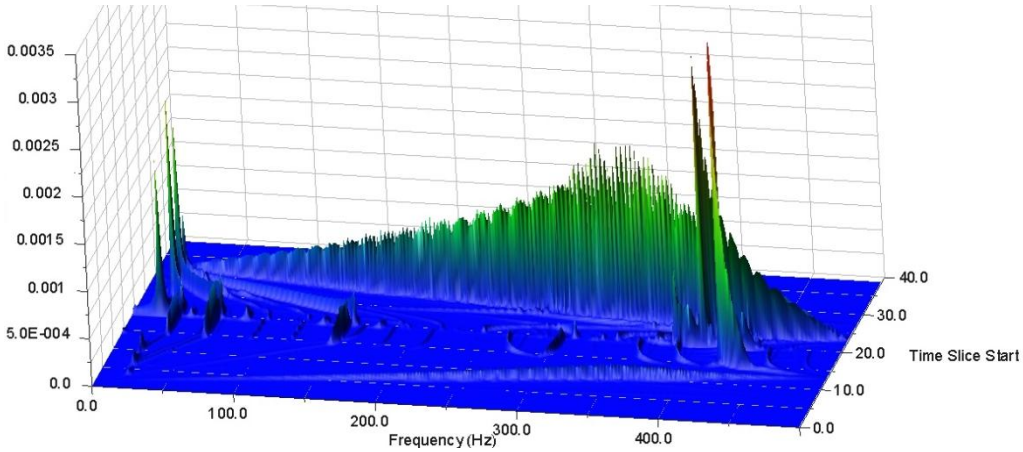

Figure 12. Waterfall spectra of High Speed gear stage deflection derivative

4 CONCLUSIONS

This study presents some features of the non-stationary dynamic behaviour of a wind turbine power train model. The model included, in a very simplified manner, some of the most important aspects that differentiate an offshore wind turbine application from an onshore application, paying particular attention to drivetrain loads. Thus, the influence of the buoy displacements on the operation of the offshore wind turbine power train was evaluated. These effects are an important difference with respect to the onshore application, and influence loads on the main bearing and planetary components as a consequence of the gyroscopic effects that appear during the star-up and emergency brake manoeuvres.

The system was analysed during two common non-stationary manoeuvres: start-up and emergency stop, revealing the influence of variable meshing stiffness on the rotational model of a power train. This meshing stiffness strongly influenced the performance of the transmission, resulting in oscillations related to the operating conditions of load and velocity.

Reversing contact (negative meshing deformation) occurred in the planetary stage at rest (time 0 sec) as a consequence of the main shaft support deflection. Moreover, during the unloaded period of the start-up operation (generator disengaged) and particularly during the emergency stop reversal, contacts were also observed between all the gear pairs. Maximum meshing deflections occurred during the braking period due to the excitation of gear train resonances.

In summary, the model presented here was found to be capable of generating plausible results in the simulation of two representative yet complex wind turbine operations, integrating the dynamics of the gearbox with the dynamics of the whole body, including the floating platform and mooring cables, in a simple and fast manner. The relevancy of the results is limited by the simplicity of the modelling methodology, and once this limitation has been qualitatively assessed based on this study, the model must be extended to include progressively higher levels of complexity, on both the buoy and drivetrain sides.

5 Acknowledgements

The authors like to thanks the company Apia XXI for supporting part of the research presented by the Project DINAER. Moreover, some parts of the developments presented have been made in the framework of Project DPI2006-14348 funded by the Spanish Ministry of Science and Technology.

6 References

[1] Sweetman, B. *Floating Offshore Wind Turbine Dynamics: Large-Angle Motions in Euler-Space*. Journal of Offshore Mechanics and Arctic Engineering, 134 (2012).
[2] Oyague, F. *Gearbox Modeling and Load Simulation of a Baseline 750-kW Wind Turbine Using State-of-the-Art Simulation Codes*, NREL/ TP-500-41160, (2009).
[3] Fernández del Rincón A., Viadero F., Pascual J., García P., Sancibrian R. *Vibration Behaviour Modelling for a Low-Speed Gearbox*, ISMA2002, (2002).
[4] A. Fernandez del Rincon, F. Viadero, M. Iglesias, P. García, A. de-Juan, R. Sancibrián, *A model for the study of meshing stiffness in spur gear transmissions*, Mechanism and Machine Theory, 61, (2013).
[5] V. K. Tamminana, S. Vijayakar and A. Kahraman, *A Study of the Relationship Between the Dynamic Factors and the Dynamic Transmission Error of Spur Gear Pairs*, Journal of Mechanical Design 129(1), (2006).
[6] V.K. Ambarisha, R.G. Parker, *Nonlinear dynamics of planetary gears using analytical and finite element models*, Journal of Sound and Vibration, 302 (2007).
[7] Peeters J. *Simulation of Dynamic Drive Train Loads in a Wind Turbine*. Dissertation. Katholieke Universiteit Leuven, (2006).
[8] Helsen J., Vanhollebeke F., Marrant B., Vandepitte D., Desmet W. *Multibody modelling of varying complexity for modal behaviour analysis of wind turbine gearboxes*, Renewable Energy, 36(11), (2011).
[9] Jonkman, J. M. *Dynamics of offshore floating wind turbines-model development and verification*, Wind Energy, 12(5), (2009).
[10] Xing, Y.H., Karimirad, M., Moan, T., *Effect of spar-type floating wind turbine nacelle motions on drivetrain dynamics*, European Wind Energy Association annual event, Copenhagen, (2012).
[11] Y. Guo, J. Keller, T. Moan, Y. Xing, *Model Fidelity Study of Dynamic Transient Loads in a Wind Turbine Gearbox*, NREL/CP-5000-58414, (2013).
[12] Kamel Abboudi, Lassad Walha, Yassine Driss, Mohamed Maatar, Taher Fakhfakh, Mohamed Haddar, *Dynamic behaviour of a two-stage gear train used in a fixed-speed wind turbine*, Mechanism and Machine Theory, 46, (2011).
[13] M.T. Khabou, N. Bouchaala, F. Chaari, T. Fakhfakh, M. Haddar, *Study of a spur gear dynamic behaviour in transient regime*, Mechanical System and Signal Processing, 25, (2011).
[14] Jason M. Jonkman, Marshall L. Buhl Jr. *FAST User's Guide, Technical Report NREL/EL-500-38230,* (2005).
[15] L. Walha, T. Fakhfakh, M. Haddar. *Nonlinear dynamics of a two-stage gear system with mesh stiffness fluctuation, bearing flexibility and backlash*, Mechanism and Machine Theory 44, (2009).
[16] Yurong Cai, *Simulation on the rotational vibration of helical gears in consideration of the tooth separation phenomenon (A new stiffness function of helical involute tooth pair)*, Journal of Mechanical Design Vol. 117, (1995).

[17] Oyague, F. *GRC Drive Train Round Robin GRC 750 / 48.2*, Loading Document IEC 61400-1 Class IIB, (2008).